frontiers | Frontiers in Materials

TYPE Original Research
PUBLISHED 18 May 2023
DOI 10.3389/fmats.2023.1137771

OPEN ACCESS

EDITED BY
Li Tao,
Beijing Institute of Technology, China

REVIEWED BY
Khosro Zangeneh Kamali,
Australian National University, Australia
Min Xi,
Chinese Academy of Sciences (CAS), China

*CORRESPONDENCE
Xinxi Li,
pkdlxx@gdut.edu.cn
Yuanwei Lin,
yuanweilin@pku.edu.cn

RECEIVED 04 January 2023
ACCEPTED 20 April 2023
PUBLISHED 18 May 2023

CITATION
Li X, Yang W, Deng J and Lin Y (2023), Surface plasmon resonance effects of silver nanoparticles in graphene-based dye-sensitized solar cells.
Front. Mater. 10:1137771.
doi: 10.3389/fmats.2023.1137771

Surface plasmon resonance effects of silver nanoparticles in graphene-based dye-sensitized solar cells

Xinxi Li[1]*, Wensheng Yang[1], Jian Deng[1] and Yuanwei Lin[2,3]*

[1]School of Materials and Energy, Guangdong University of Technology, Guangzhou, China, [2]Beijing National Laboratory for Molecular Sciences, State Key Laboratory for Structural Chemistry of Unstable and Stable Species, College of Chemistry and Molecular Engineering, Peking University, Beijing, China, [3]Center for Nanoscience and Nanotechnology, Academy for Advanced Interdisciplinary Studies, Peking University, Beijing, China

Localized surface plasmon resonance (LSPR) has been applied in photovoltaic devices to improve their photoelectric conversion efficiency. In this study, the mechanism of LSPR in dye-sensitized solar cells (DSSCs) was determined. Specifically, silver nanoparticles were formed by evaporating silver in electro-beam equipment and then annealing it in a tube furnace. The sizes of the nanoparticles varied with the changes in their thicknesses during evaporation and annealing. A DSSC-based graphene was designed to consist of different sizes of metal nanoparticles assembled on a cathode electrode. The photon electric performance of the DSSCs, which depended on Ag nanoparticles, was analyzed in detail, with a particular focus on nanoparticle size. Compared with the DSSC without Ag nanoparticles, the DSSC with LSPR exhibited excellent electric current density and incident photon-to-current efficiency (IPCE) performance due to the LSPR effect. The DSSC assembled with 10 nm-thick Ag film and annealed to form nanoparticles exhibited a high IPCE of 70.03%. The IPCE value of this DSSC was 45.15% higher than that of the pure graphene-based DSSC (31.62%). However, Ag nanoparticles increased to a certain degree and became aggregated and concatenated, thereby decreasing the LSPR effect on DSSCs. Therefore, LSPR plays an important role in the photon-electrical performance of DSSCs.

KEYWORDS

localized surface plasmon resonance, dye-sensitized solar cell, graphene, silver nanoparticles, energy materials

1 Introduction

The localized surface plasmon resonance (LSPR) of nanoparticles has attracted significant attention in different applications, such as optical antennas (You et al., 2022), surface enhanced Raman spectrophotometry (Gu et al., 2022), and titanium oxide photocatalysts (Andronic et al., 2022). When metal nanoparticles absorb incident light, the radiated light scatters around the particle surface, and a strong electromagnetic field is generated by an evanescent wave (Hasan et al., 2022). The nanoparticle surface is localized by the electromagnetic field, which maintains a distance of less than the diameter of the nanoparticle.

LSPR enhancement is affected by many factors, such as particle size, particle shape, incident light wavelength, dielectric constant of materials, and surface state of particles (Hu

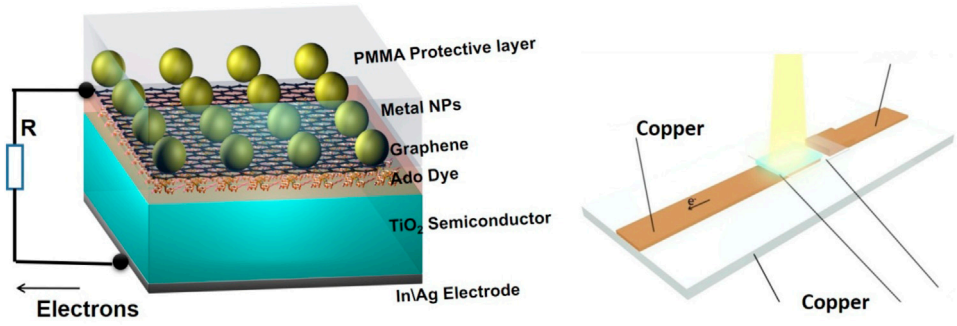

FIGURE 1
Schematic of the device structure.

et al., 2022; Kim and Ha, 2022; Zhu et al., 2022; Zhu and Zhao, 2022). The LSPR of metal nanoparticles is recognized as an effective approach to improve the performance of photoelectric devices due to its important advantages (Ninawe and Dhawan, 2022; Rasheed and Sayidmarie, 2022).

In recent years, the enhancement of dye-sensitized solar cells (DSSCs) by surface plasmon has been reported (Dahlan et al., 2022; Zhang et al., 2022). DSSCs can display some advantages such as low-cost fabrication, semi-transparency, and environment friendliness. Thus, DSSCs have been regarded as a suitable source of electrical energy in future solar cells. Gratzel proposed mesoporous titanium dioxide (TiO_2) films and ruthenium sensitizers to improve the efficiency of DSSCs (O'Regan and Grätzel, 1991). The energy conversion efficiencies of DSSCs should be efficiently improved to make them feasible and economical photovoltaic devices. In fact, the energy conversion efficiency of DSSCs is affected by many factors, such as the energetic suitability of HOMO-LUMO levels (Badawy et al., 2022; Majid et al., 2022), available large surface areas for the dye (Siddika et al., 2022), transport kinetics of electrons (Koshika et al., 2022), and losses due to electron hole recombination and back reactions (Bouwens et al., 2022).

Many researchers have designed different DSSCs, such as various photosensitive substances (Stavitskaya et al., 2022), electrolytes (Bashir et al., 2022), and nanostructures (Salimian et al., 2022), to improve their photon conversion efficiency.

Several approaches have been used to improve the efficiency of DSSCs. One approach is the absorption of ultra-visible and far infrared light to excite the dye and generate many photo-simulated carriers. The electrons are injected into the semiconductor layer. Thus, enhancing the light-harvesting efficiency of the dye is the most effective method to improve the efficiency of DSSCs. LSPR has been applied in various photovoltaic devices, such as organic solar cells (Ike et al., 2022), thin film silicon solar cells (Zarerasouli et al., 2022), quantum dot photovoltaics (Kim et al., 2022), and DSSCs (Kaur et al., 2022). LSPR effectively improves the solar conversion efficiency of DSSCs by producing a strong electromagnetic field near the surface of metal nanoparticles and enhancing the light absorption force of the dye in the visible range of wavelengths.

The interface mechanisms between the metallic nanostructure and dielectric layer of the designed photovoltaic device have been studied in our previous research. The substrate induced plasmon concentrated light at the interface, enhanced the photo-excitation of dyes, and improved the photoelectric conversion (Li et al., 2015). In the current research, a DSSC-based graphene consisting of different sizes of evaporated metal nanoparticles is designed. The basic structure of this DSSC is shown in Figure 1. Given the metal nanoparticles with LSPR, the dye is stimulated by the electromagnetic field to improve the efficiency of DSSCs. To investigate the effects of Ag NP-modified DSSCs with various sizes, we adopt different physical, optical, and electrical measurement techniques.

2 Experimental and schematic

2.1 Graphene growth

A low-pressure chemical vapor deposition method with methane was utilized to produce a high-quality, single-layer graphene with a carbon-containing precursor under optimal conditions (Sun et al., 2021). The substrate of the graphene was copper foil, which was initially pretreated with acetic acid and then posited in a split tube furnace to produce the graphene. During graphene growth, the foil was annealed at a temperature of 1,045°C under 10 sccm H_2 flow for 60 min and then for 15 min. The temperature rapidly dropped to room temperature under hydrogen protection.

2.2 Preparation of metal nanoparticles

Ag alloy thin films with proportional silver volume ratios and thicknesses were evaporated on the surface of the graphene on the copper foil substrate under the condition of 0.1 Å/s and a pressure of 2×10^{-4} Pa. Then, the films were annealed at 300°C for 30 min under H_2 (600 sccm) and Ar (600 sccm) as protective gas atmospheres. As a result, silver nanoparticles formed on the graphene surface. The graphene film deposited silver films, namely, Gr + Ag5, Gr + Ag10, Gr + Ag15, and Gr + Ag20 with sizes of 5, 10, 15, and 20 nm, respectively. The thicknesses of the Ag films deposited on the graphene increased with the increase of annealing time, and the sizes of the Ag nanoparticles after annealing increased

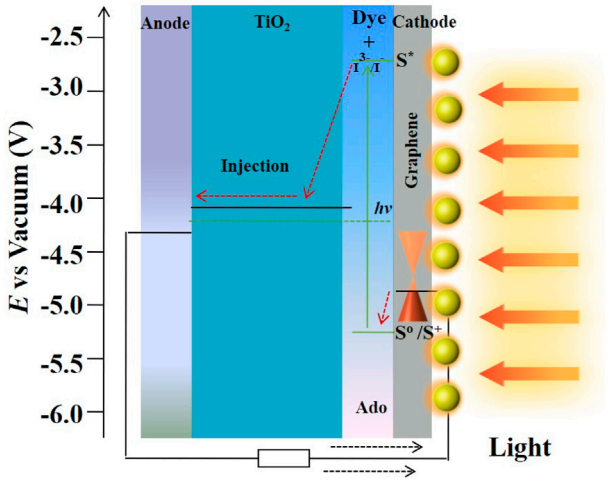

FIGURE 2
Schematic of the mechanism effect of the designed DSSC.

correspondingly. These metal nanoparticles play an important role in the incident photon-to-current efficiency (IPCE) and charge transfer properties of DSSCs.

2.3 Back electrode/TiO_2/Ado/electrolyte layer preparation

Rutile TiO_2 (001) single crystals were purchased from MTI Corporation. Each crystal exhibited a mechanically polished side and an atomically flat surface. A 100 nm In and a 100 nm Ag were evaporated on the rough back side of the TiO_2 crystals. Before the assembly of the Ado molecule dye to the semiconductor, TiO_2 (001) was crossed for chemical polishing by an aqueous HF solution (30% HF, 1 min) and was etched with oxygen plasma (15 Pa, 30 W; 1 min) for surface hydroxyl activation. Then, the Ado molecule was assembled on TiO_2 by immersing the samples in a 10 mg/mL solution of Ado in water for 48 h. An iodide-triiodide (I/I_3^-)-based redox electrolyte that contained 0.5 M of LiI, 0.05 M of I_2, 0.5 M of 4-tert-butylpyridine, and 0.5 M of 1-butyl-3-methylimidazolium iodide in acetonitrile was injected in the vacant space. The In/Ag side of the samples was fixed on a copper foil using a special conductive tap, and the back electrode was sealed with epoxy (Epotek 377) and then dried for at least 40 min to solidify.

2.4 SLG/NP layer formation

For the assembly of the SLG/NP layer, the poly(methyl methacrylate) (PMMA) (MicroChem 950 PMMA A6) layer was spined cast on the surface of the SLG/NP samples on copper under the condition of 4,000 revolutions per minute (rpm) for 30 s and was then heated to 180°C for 3 min. Considering that the two sides of the copper foils showed graphene growth, we etched the back side of SLG/NP/PMMA samples by oxygen plasma to remove residual graphene.

Moreover, the copper layer in the back samples was wet eroded in a 1 M $(NH_4)_2S_2O_8$ aqueous solution for 8 h to produce an SLG/NP/PMMA film that should float on the surface of the solution. Then, the floating film was fetched by tweezers and was repeatedly washed using copious amounts of ultrapure water and isopropanol. Finally, the SLG/NP/PMMA sample was transferred on the dye layer.

2.5 Schematic of DSSC

The schematic of the structure of a DSSC is displayed in Figure 1. Figure 2 illustrates the schematic of the mechanism of the designed graphene-based DSSC device. The metal nanoparticles absorbed incident light and generated LSPR. The energy generated by the nanoparticles through the graphene was transported to the semiconductor surface, and the absorbed Ado molecule was excited on the TiO_2 layer. At the same time, the I_3^-/I^- electrolyte prompted the separation of electrons and holes, and electron and hole pairs were generated. The photoactivated electrons through the semiconductor were transported to the back electrode with Ohmic contacts for collection. Meanwhile, the photoactivated holes were transferred to the graphene layer for collection. In sum, the back-metal electrode as a photoanode and graphene as a photocathode were externally connected to form a circuit and achieve photoelectric conversion.

2.6 Morphology characterizations

The morphology characterizations of metal nanoparticles were investigated by using a field-emission scanning electron microscope (FE-SEM; Hitachi Limited, S4800). The elemental composition and crystal structure of the nanoparticles were evaluated by using a high-resolution transmission electron microscope (HRTEM; FEI, Tecnai F30). The energy dispersive X-ray (EDX) analysis of the nanoparticles revealed the presence of elements in the nanoparticles.

2.7 Photovoltaic performance evaluation

The power conversion parameters of the single graphene and Ag NP DSSC were measured by using a solar simulator with a light intensity of 100 mW/cm^2 calibrated at AM 1.5 with a digital source meter (Science Tech). The current–voltage characteristics of the photovoltaic devices were measured by using a semiconductor characterization system (Agilent 4155C). Serial parameters, such as short circuit current density (Jsc) and incident optical power (Pin), were used to analyze the power conversion efficiency of the single graphene and Ag NP-based DSSC.

2.8 IPCE calculation

For the IPCE spectroscopic measurements, a computer-controlled grating monochromator (Zolix Omni-λ150) with a

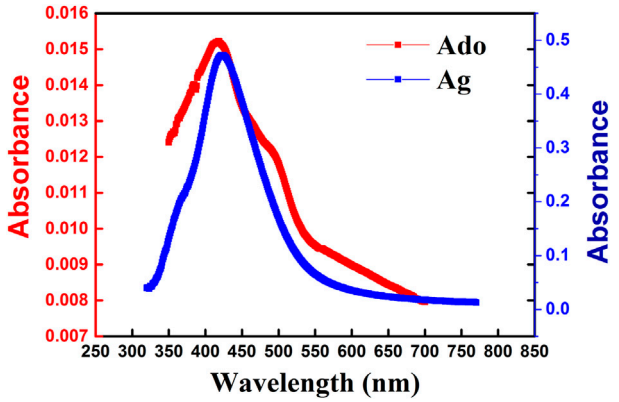

FIGURE 3
Extinction spectra of PMMA-supported graphene and Ag-NP film on Ado molecular layer assembled on TiO_2 substrate.

150 W Xe lamp was used to provide monochromatic light illumination to the samples with an optical filter. The corresponding wavelength of monochromatic light illumination was measured by an OPT-2000 spectrophotometer. The corresponding photocurrent was measured with an Agilent 4155C semiconductor parameter analyzer at current time mode. The IPCE was calculated from the measured photocurrents and corresponding monochromatic light wavelength (λ). The following formula was used to expressed IPCE.

$$\mathrm{IPCE} = \frac{\mathrm{hc}}{\lambda}\left[\frac{photocurrents\left(\frac{nA}{cm^2}\right)}{light\ power\left(\frac{nW}{cm^2}\right)}\right]$$

where *h is* the Planck's constant and *c* is the speed of light. In this research, all the photoelectrical results were measured by using three samples.

3 Results and discussion

3.1 Physical characterization and analysis

3.1.1 UV-visible spectroscopy

The pure Gr and Ag-Gr photocathode samples were tested in the range of 300–800 nm. As displayed in Figure 3, the peak curve of the Gr + Ag10 extinction spectrum is apparent at 428 nm, and the Ado molecule absorption peak position is about 415 nm. This value nearly matched the absorption peak of Ado on the TiO_2 surface. This condition embodied the effect of surface plasmon resonance that enhanced the incident light utilization.

The light absorption enhancement was attributed to the LSPR effect, which created a strong electromagnetic field around the Ag NP and produced an effective resonant energy transfer to the adopted dye on the semiconductor (Mathew and Shyju, 2022). Therefore, Ag NPs are effective for visible light response.

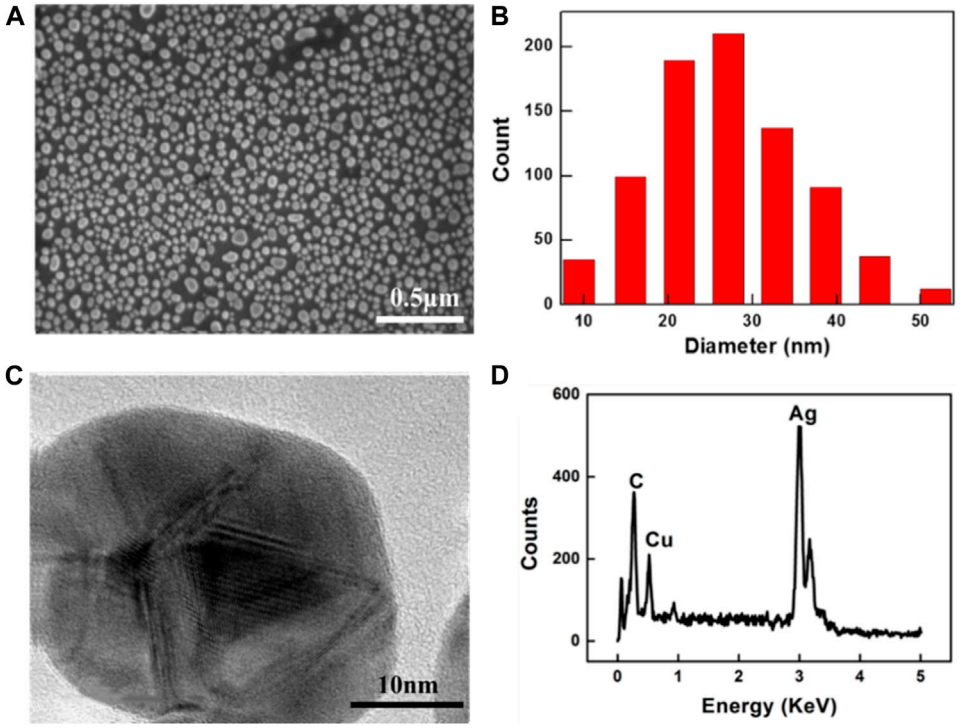

FIGURE 4
Characteristic of Ag nanoparticles: **(A)** FE-SEM image of Ag nanoparticles annealed by 10 nm Ag film, **(B)** the size distribution histogram of Ag nanoparticles, **(C)** HRTEM image of single Ag nanoparticles, and **(D)** EDX analysis of Ag nanoparticles.

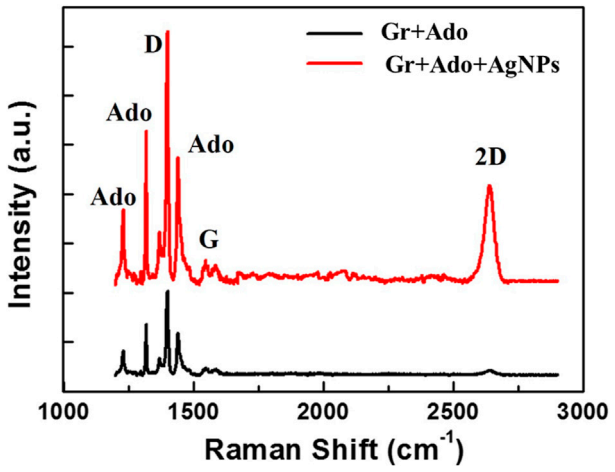

FIGURE 5
Raman spectra of samples: Raman spectra of Ado on Gr and Ado on Gr/Ag nanoparticles.

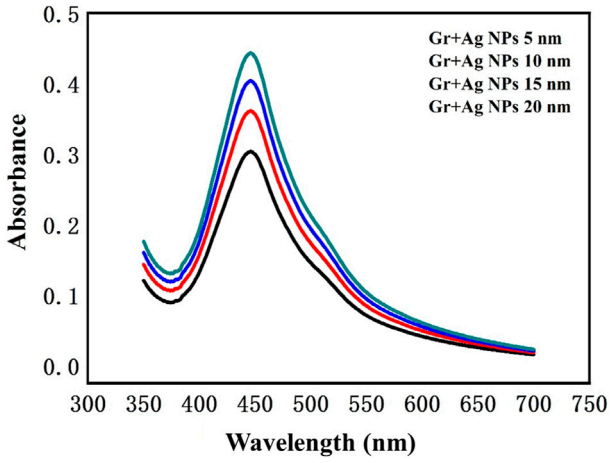

FIGURE 6
Extinction spectra of silver nanoparticles with different diameters and sizes after annealing.

3.1.2 Physical characteristics of silver nanoparticles

As shown in Figure 4A, silver nanoparticles were annealed on ten nm-thick silver film and were thermally evaporated on a single layer graphene surface, which were formed on graphene uniformly. The SEM images indicates that the silver nanoparticles exhibited even distribution, with their average diameter are about 42.1 nm, as shown in Figure 4B. The results of HRTEM and EDX characterization of the silver nanoparticles are displayed in Figures 4C, D, respectively. The lattice distance and facet of the pure silver nanoparticles were approximately 2.35 Å and (111). The EDX dispersive peaks obviously displayed the silver element, so it can be induced that Ag NPs were well-assembled on graphene.

3.1.3 Raman spectroscopy of silver nanoparticles

The Raman spectroscopy of graphene assembled with Ado and silver nanoparticles is shown in Figure 5. For the Raman spectrum of pure graphene, the small G/2D ratio, narrow single symmetric 2D peak (−2,694 cm^{-1}), and negligible D peak indicated that graphene comprised a single layer and exhibited relatively high quality (Thapliyal et al., 2022). The D peak indicated that graphene comprised a single layer and showed high quality. However, for the graphene assembled with silver nanoparticles, it can display only the D peak of 1,353 cm^{-1} is noted, it reveals the small damage on graphene during the formation of silver nanoparticles, and the formation of silver nanoparticles on the graphene surface causes negligible damage on the graphene layer (Bayle et al., 2015). The peaks of Ado at 1,200–1,650 cm^{-1} in the Raman spectra of the Ado/SLG/NP samples were significantly enhanced compared with those in the spectra of Ado on pure graphene. This finding indicated that silver NPs converged light to the Ado layer below the graphene (Suo et al., 2021).

3.2 Physical analysis of silver nanoparticles with different diameter sizes

3.2.1 Extinction of silver nanoparticles with different diameter sizes

UV-vis spectroscopy has been adopted to evaluate the quantity of nanoparticles among different samples. As displayed in Figure 6, the absorbance of the silver nanoparticles with different thicknesses is compared. The main reason is that the free electrons of the metal nanoparticles are in resonant with incidence of photons. As shown in Figure 6, the absorption peak amplitudes increased correspondingly with the increase of the size of the Ag nanoparticles. The absorbance intensity gradually increased when the thickness of the silver film increased from 5 nm to 20 nm. Meanwhile, the absorption peak presented a blue shift. The increased absorption peak can significantly enhance the peaks of the samples accompany with the increasing size of the metal nanoparticle. Therefore, the surface plasmon resonance correspondingly changed with the changes in the size of the Ag nanoparticles.

3.2.2 SEM characterization of silver nanoparticles with different thicknesses

The suitable size, proper morphology, and relatively high specific surface area of metal nanoparticles benefit the generation of sufficient energy by LSPR. Figure 7 shows the FE-SEM images of different Ag nanoparticles. The obtained Ag nanoparticles showed a uniform distribution when the thickness of the silver film increased from 5 nm to 10 nm. This condition should be contributed to the LSPR effect. However, the sizes of the silver nanoparticles after annealing became aggregated when the thickness of the evaporated silver film surpassed to 15 nm. This condition rapidly decreased the LSPR effect.

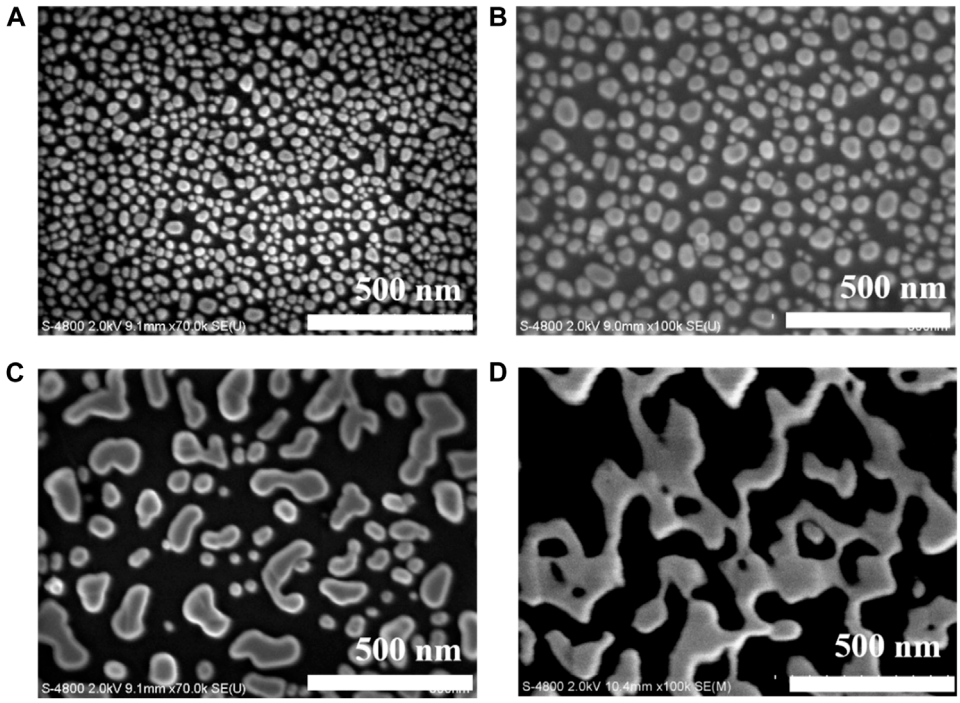

FIGURE 7
FE-SEM of different silver nanoparticles. **(A)** Gr + Ag5, **(B)** Gr + Ag10, **(C)** Gr + Ag15, and **(D)** Gr + Ag20.

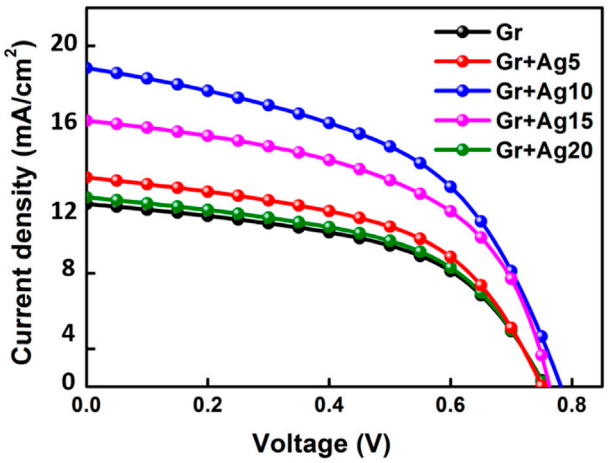

FIGURE 8
Current–voltage characteristic of different DSSCs containing pure Gr, Gr + Ag5, Gr + Ag10, Gr + Ag15, and Gr + Ag20.

TABLE 1 Performance of pure Gr, Gr + Ag5, Gr + Ag10, Gr + Ag15, and Gr + Ag20 DSSCs.

Samples	Jsc (mA·cm^{-2})	Voc (V)	FF (%)	η (%)
Pure Gr	12.2	0.73	53.6	5.13
Gr + Ag5	14.3	0.73	53.7	6.26
Gr + Ag10	19.2	0.77	51.6	7.52
Gr + Ag15	16.1	0.76	52.3	6.64
Gr + Ag20	12.6	0.74	53.6	5.27

3.3 Electrical characterization of DSSCs

3.3.1 J-V characteristic

The photovoltaic performance and efficiency of different DSSCs, such as pure Gr, Gr + Ag5, Gr + Ag10, Gr + Ag15, and Gr + Ag20, were tested by a semiconductor characterization system under standard conditions (1 Sun; input power of 100 mW cm^2; AM 1.5). The current–voltage curves are displayed in Figure 8. The Jsc, open-circuit voltage (Voc), fill factor (FF), IPCE, and photon-to-current efficiency (PCE) (η) among different solar cells were calculated using a solar simulator when sunlight was simulated on an active area of 0.15 cm^2. The relative data are tabulated in Table 1.

In the present work, Gr + Ag10 DSSC exhibited a relatively high PCE of 7.52%, which was obviously higher than that of the pure Gr sample. The 10 nm Gr + Ag10 displayed a suitable particle size and proper particle distance, which increased the absorbance of incident light and enhanced the SPR effect. However, the nanoparticles began to aggregate and decreased the LSPR effect when the size of the silver particles surpassed a certain degree. For example, in this study, silver nanoparticles formed after annealing of a 15 nm thick Ag film are prone to aggregation due to their larger size, which minimizes energy transfer to the dye. Therefore, the Jsc of DSSC decreased when the metal nanoparticles increased to a certain degree.

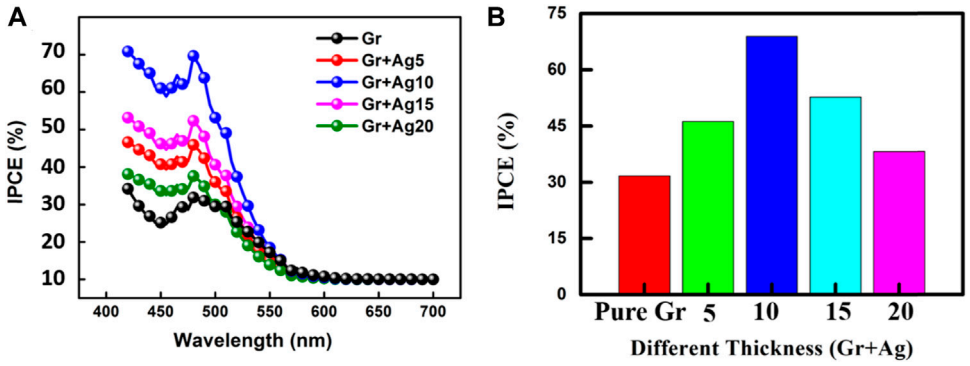

FIGURE 9
IPCE values of different DSSCs containing different Ag nanoparticles, such as pure Gr, Gr + Ag5, Gr + Ag10, Gr + Ag15, and Gr + Ag20: **(A)** IPCE spectra of different DSSCs and **(B)** IPCE values of different DSSCs.

3.3.2 IPCE performance of different DSSCs

The IPCE spectra of pure Gr, Gr + Ag5, Gr + Ag10, Gr + Ag15, and Gr + Ag20 are shown in Figure 9. The IPCE values of Gr + Ag5 and Gr + Ag10 improved, whereas those of Gr + Ag15 and Gr + Ag20 did not. This result was due to the serious aggregation of the nanoparticles and the increased recombination between electrons. The electron injection and charge transfer efficiency increased correspondingly with the increase of Ag film thickness (Di and Qin, 2022).

As shown in the analysis in Figure 9, the IPCE of pure G-based DSSC was 31.62%, and the IPCE of Gr + Ag10 DSSC was approximately 70.03%, which indicated significant improvement due to the silver nanoparticles. The improvement of electron injection and charge transfer efficiency was mainly due to the deposition of the Ag nanoparticles on graphene that increased the LSPR effect. Thus, the IPCE of DSSC increased correspondingly. However, the Ag nanoparticles began to aggregate and concatenate and decreased the LSPR effect when they were increased to a certain degree, such as the case of Gr + Ag15. Therefore, the IPCE values of different DSSCs containing different Ag nanoparticles decreased after the modification of Ag nanoparticles to a certain degree.

Considering the above analysis, the size of the metal nanoparticles is one of the important parameters to the magnitude of the plasmon enhancement effect. Concentrated energies with a strong electromagnetic field were produced by the metal nanoparticles in the DSSCs, and the SPR effect enhanced the incident light scattering and increased the optical path length and Jsc. Meanwhile, the improvement of photo electron generation increased the IPCE. However, the metal nanoparticles began to aggregate and concatenate when their size was increased to a certain degree. The condition decreased the LSPR effect.

3.3.3 Electrochemical impedance spectroscopy of different silver nanoparticles with modified graphene samples

The IPCE values for different DSSCs, such as pure Gr, Gr + Ag5, Gr + Ag10, Gr + Ag15, and Gr + Ag20, were investigated. The IPCE values of the DSSCs decreased with the increase in silver nanoparticles to a certain degree. This result was contrary to the incident light absorption. To identify this phenomenon, we measured the internal impedance of the DSSCs.

TABLE 2 Obtained EIS parameters from fitting Nyquist plots of DSSCs containing Ag nanoparticles of different sizes.

Samples	Rt (Ω)	Rr (Ω)	Rd (Ω)	Jsc (mA)
Pure Gr	2.65	30.13	5.02	12.1
Gr + Ag5	2.39	32.89	6.12	14.3
Gr + Ag10	2.13	41.32	6.37	19.2
Gr + Ag15	2.43	39.58	5.75	16.1
Gr + Ag20	2.61	31.06	5.31	12.6

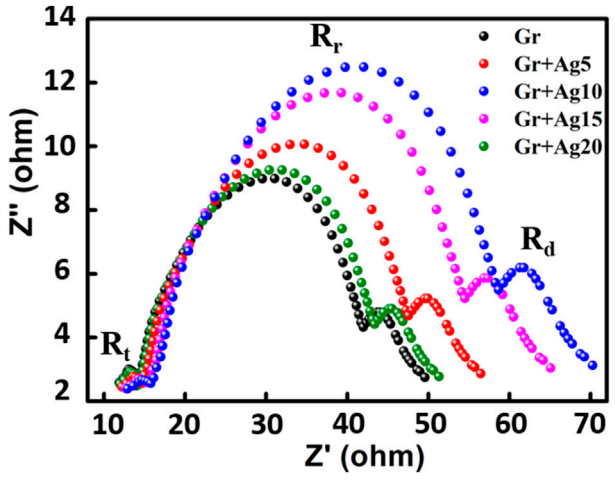

FIGURE 10
Nyquist plots of EIS for different DSSCs, namely, pure Gr, Gr + Ag5, Gr + Ag10, Gr + Ag15, and Gr + Ag20.

The EIS parameters are summarized in Table 2, and the corresponding diagrams for the DSSCs with and without metal nanoparticles are shown in Figure 10.

The photo-electrode/dye/electrolyte interface focused on the LSPR effect during the charge transfer process. In Figure 10, three semicircles, namely, Rt, Rr, and Rd, denote transport, recombination, and diffusion resistances, respectively (Dhonde et al., 2017). Charge resistance (Rt) and recombination resistance (Rr) were affected by the LSPR of the silver nanoparticles. The first semicircle Rt that corresponded to a high frequency range presented charge transfer resistance. The increase of the middle semicircle Rr indicated a high value of charge recombination resistance accompanied by an increased charge transfer mechanism. Thus, the PCE increased correspondingly (Bhojanaa et al., 2020; Selvapriya et al., 2022). For the Gr + Ag10 sample, the Rt and Rr values were observed to be 2.13 and 41.32 Ω, respectively. Thus, these findings are very in agreement with the J-V results of DSSCs.

4 Conclusion

In this study, a DSSC with TiO_2/Dye/SLG/NP structure was designed to investigate the effects of LSPR enhancement on photovoltaic conversion. The DSSC with LSPR exhibited excellent electric current density and IPCE performance relative to the DSSC without Ag nanoparticles due to the LSPR effect. For the DSSC assembled with 10 nm-thick Ag film and annealed to form nanoparticles, Gr + Ag10 obtained the highest IPCE of 70.03%, which was 45.15% higher than that of pure Gr (31.62%). Therefore, the suitable quantity of Ag nanoparticles played an important role in enhancing the photon electric conversion efficiency due to the LSPR effect. The proper proportion of metal nanoparticles represents a valuable and efficient method for improving the performance of DSSCs.

Data availability statement

The original contributions presented in the study are included in the article/Supplementary Material, further inquiries can be directed to the corresponding authors.

Author contributions

XL and YL designed and conducted the whole project. WY and JD performed the experiments and wrote the first draft of the manuscript. XL and YL revised the manuscript, and all the authors made contribution to the data analysis.

Funding

This work is financially supported by the National Natural Science Foundation of China (21875046 and 51803036), and the Guangzhou emerging industry development fund project of Guangzhou development and reform commission (2018841).

Conflict of interest

The authors declare that the research was conducted in the absence of any commercial or financial relationships that could be construed as a potential conflict of interest.

Publisher's note

References

Andronic, L., Lelis, M., Enesca, A., and Karazhanov, S. (2022). Photocatalytic activity of defective black-titanium oxide photocatalysts towards pesticide degradation under UV/VIS irradiation. *Surfaces Interfaces* 32, 102123. doi:10.1016/j.surfin.2022.102123

Badawy, S. A., Abdel-Latif, E., Fadda, A. A., and Elmorsy, M. R. (2022). Synthesis of innovative triphenylamine-functionalized organic photosensitizers outperformed the benchmark dye N719 for high-efficiency dye-sensitized solar cells. *Sci. Rep.* 12, 12885. doi:10.1038/s41598-022-17041-1

Bashir, S., Iqbal, J., Farhana, K., Jafer, R., Hina, M., Kasi, R., et al. (2022). "Chapter 9 - hybrid organic polymer electrolytes for dye-sensitized solar cells," in *Dye-sensitized solar cells*. Editors A. K. Pandey, S. Shahabuddin, and M. S. Ahmad (Massachusetts, United States: Academic Press), 181–212.

Bayle, M., Reckinger, N., Huntzinger, J., Felten, A., Bakaraki, A., Landois, P., et al. (2015). Dependence of the Raman spectrum characteristics on the number of layers and stacking orientation in few-layer graphene. *Phys. status solidi (b)* 252, 2375–2379. doi:10.1002/pssb.201552204

Bhojanaa, K. B., Ramesh, M., and Pandikumar, A. (2020). Complementary properties of silver nanoparticles on the photovoltaic performance of titania nanospheres based photoanode in dye-sensitized solar cells. *Mater. Res. Bull.* 122, 110672. doi:10.1016/j.materresbull.2019.110672

Bouwens, T., Bakker, T. M. A., Zhu, K., Hasenack, J., Dieperink, M., Brouwer, A. M., et al. (2022). Using supramolecular machinery to engineer directional charge propagation in photoelectrochemical devices. *Nat. Chem.* 15, 213–221. doi:10.1038/s41557-022-01068-y

Dahlan, D., Umar, M. I. A., Sadikin, S. N., Ridwan, J., and Umar, A. A. (2022). Photoelectrical process uplift in Mg-doped-TiO2 photoanode of dye-sensitized solar cells. *Opt. Mater.* 133, 112976. doi:10.1016/j.optmat.2022.112976

Dhonde, M., Sahu, K., Murty, V. V. S., Nemala, S. S., and Bhargava, P. (2017). Surface plasmon resonance effect of Cu nanoparticles in a dye sensitized solar cell. *Eelctrochimica Aata* 249, 89–95. doi:10.1016/j.electacta.2017.07.187

Di, Y., and Qin, T. (2022). Plasmonic ZrN@TiO2 core-shell nanostructure enhancing photovoltaic performance of dye-sensitized solar cells. *Opt. Mater.* 132, 112813. doi:10.1016/j.optmat.2022.112813

Gu, Y., Li, Q., Yin, M., Yang, D., and Yang, Y. (2022). A super-hydrophobic perfluoropolyether coated polytetrafluoroethylene sheets substrate for detection of acetamiprid surface-enhanced Raman spectroscopy. *Spectrochimica Acta Part A Mol. Biomol. Spectrosc.* 278, 121373. doi:10.1016/j.saa.2022.121373

Hasan, A. S., Alwahib, A. A., and Al-azawi, R. J. (2022). Review of surface plasmon resonance phenomenon applied in different applications. *AIP Conf. Proc.* 2660, 20129.

Hu, J., Chen, Y., Li, J., Ma, Y., and Shu, C. (2022). Geometrical parameter effect on plasmonic scattering of bimetallic three-layered nanoshells. *Nanomaterials* 12, 3816. doi:10.3390/nano12213816

Ike, J. N., Hamed, M. S. G., and Mola, G. T. (2022). Effective energy harvesting in thin film organic solar cells using Ni:Zn as bimetallic nanoparticles. *J. Phys. Chem. Solids* 161, 110405. doi:10.1016/j.jpcs.2021.110405

Kaur, N., Singh, D. P., and Mahajan, A. (2022). Plasmonic engineering of TiO2 photoanodes for dye-sensitized solar cells: A review. *J. Electron. Mater.* 51, 4188–4206. doi:10.1007/s11664-022-09707-3

Kim, G. W., and Ha, J. W. (2022). Single-particle study on Hg amalgamation mechanism and slow inward diffusion in mesoporous silica-coated gold nanorods without structural deformation. *J. Phys. Chem. Lett.* 13, 2607–2613. doi:10.1021/acs.jpclett.2c00189

Kim, S., Park, T., Oh, G., Kim, B., Ju, Y. S., and Rho, W. (2022). Structural transition of gold octahedrons to nanoprisms induced by nitrogen-doped carbon quantum dots. *Colloid Interface Sci. Commun.* 51, 100675. doi:10.1016/j.colcom.2022.100675

Koshika, M., Cho, I., Yoshii, N., Yoshimura, K., Morikawa, D., Takagi, R., et al. (2022). Molecular geometry dependent electronic coupling and reorganization energy for electron transfer between dye molecule adsorbed on TiO2 electrode and Co complex in electrolyte solutions. *J. Phys. Chem. C* 126, 3339–3350. doi:10.1021/acs.jpcc.1c09343

Li, X., Jia, C., Ma, B., Wang, W., Fang, Z., Zhang, G., et al. (2015). Substrate-induced interfacial plasmonics for photovoltaic conversion. *Sci. Rep.* 5, 14497. doi:10.1038/srep14497

Majid, A., Kiran, S., Sandhu, Q., Khan, S., and Khan, S. (2022). The effects of polar solvents on structural, electronic, and optical properties of organic dyes. *Int. J. Quantum Chem.* 122, e26876. doi:10.1002/qua.26876

Mathew, J., and Shyju, T. S. (2022). Plasmon-enhanced efficiency of DSSC and hybrid nano catalysis applications. *Top. Catal.* 65, 1719–1732. doi:10.1007/s11244-022-01678-3

Ninawe, A., and Dhawan, A. (2022). Numerical investigation of plasmonic bowtie nanorings with embedded nanoantennas for achieving high SEIRA enhancement factors. *Mater. Res. Express* 9, 96201.

O'Regan, B., and Grätzel, M. (1991). A low-cost, high-efficiency solar cell based on dye-sensitized colloidal TiO2 films. *Nature* 353, 737–740. doi:10.1038/353737a0

Rasheed, A. A., and Sayidmarie, K. H. (2022). "Absorption enhancement and scattering inhibition for Bowtie Nanoantenna," in 2022 IEEE 9th International Conference on Sciences of Electronics, Technologies of Information and Telecommunications (SETIT), Hammamet, Tunisia, 28-30 May 2022, 75–80.

Salimian, J., Osfouri, S., Azin, R., and Jalali, T. (2022). Impacts of paste preparation methods on the porous TiO2 nanostructure properties and naturally dye-sensitized solar cells performance. *J. Mater. Res. Technol.* 18, 4816–4833. doi:10.1016/j.jmrt.2022.04.134

Selvapriya, R., Abhijith, T., Ragavendran, V., Sasirekha, V., Reddy, V. S., Pearce, J. M., et al. (2022). Impact of coupled plasmonic effect with multishaped silver nanoparticles on efficiency of dye sensitized solar cells. *J. Alloys Compd.* 894, 162339. doi:10.1016/j.jallcom.2021.162339

Siddika, A., Sultana, M., Bashar, M. S., Tabassum, S., Aziz, S., and Ali Shaikh, M. A. (2022). Improved performance of dye sensitized solar cell by exploration of photoanode and ruthenium based dye. *Opt. Mater.* 125, 112042. doi:10.1016/j.optmat.2022.112042

Stavitskaya, A., Khusnetdenova, E., Vinokurov, V., Lvov, Y., and Fakhrullin, R. (2022). Prokaryotic and eukaryotic toxicity of halloysite decorated with photoactive nanoparticles. *Chem. Commun.* 58, 7719–7729. doi:10.1039/d2cc02439j

Sun, B., Pang, J., Cheng, Q., Zhang, S., Li, Y., Zhang, C., et al. (2021). Synthesis of wafer-scale graphene with chemical vapor deposition for electronic device applications. *Adv. Mater. Technol.* 6, 2000744. doi:10.1002/admt.202000744

Suo, H., Yang, S., Ji, P., and Wang, Y. (2021). Multi-band enhanced graphene photodetector based on localized surface plasmon. *Sensors Actuators A Phys.* 322, 112627. doi:10.1016/j.sna.2021.112627

Thapliyal, V., Alabdulkarim, M. E., Whelan, D. R., Mainali, B., and Maxwell, J. L. (2022). A concise review of the Raman spectra of carbon allotropes. *Diam. Relat. Mater.* 127, 109180. doi:10.1016/j.diamond.2022.109180

You, Q., Li, Z., Li, Y., Qiu, L., Bi, X., Zhang, L., et al. (2022). Resonance photoluminescence enhancement of monolayer MoS2 via a plasmonic nanowire dimer optical antenna. *ACS Appl. Mater. Interfaces* 14, 23756–23764. doi:10.1021/acsami.2c02684

Zarerasouli, P., Bahador, H., and Heidarzadeh, H. (2022). Performance improvement of an ultra-thin film solar cell based on optimized CIGS (Cu(In1-x, Gax)Se2) using appropriate plasmonic nanoparticles. *Opt. Mater.* 131, 112729. doi:10.1016/j.optmat.2022.112729

Zhang, X., Fan, R., Liu, M., Cao, Y., Sun, P., Zhang, Y., et al. (2022). Preparation of CoNi@CN composites based on metal-organic framework materials as high efficiency counter electrode materials for dye-sensitized solar cells. *Sol. Energy* 231, 767–774. doi:10.1016/j.solener.2021.12.006

Zhu, J., and Zhao, S. (2022). Improve the effective resonance light scattering of three-layered plasmonic Au@dielectric@Ag bimetallic nanoshells. *Plasmonics* 17, 173–180. doi:10.1007/s11468-021-01510-w

Zhu, S., Zhao, Q., Fu, H., Zhang, H., Bao, H., Le, Z., et al. (2022). Chemical interface damping-induced attenuation of surface plasmon-enhanced Raman spectroscopy. *ACS Photonics* 9, 3000–3011. doi:10.1021/acsphotonics.2c00685